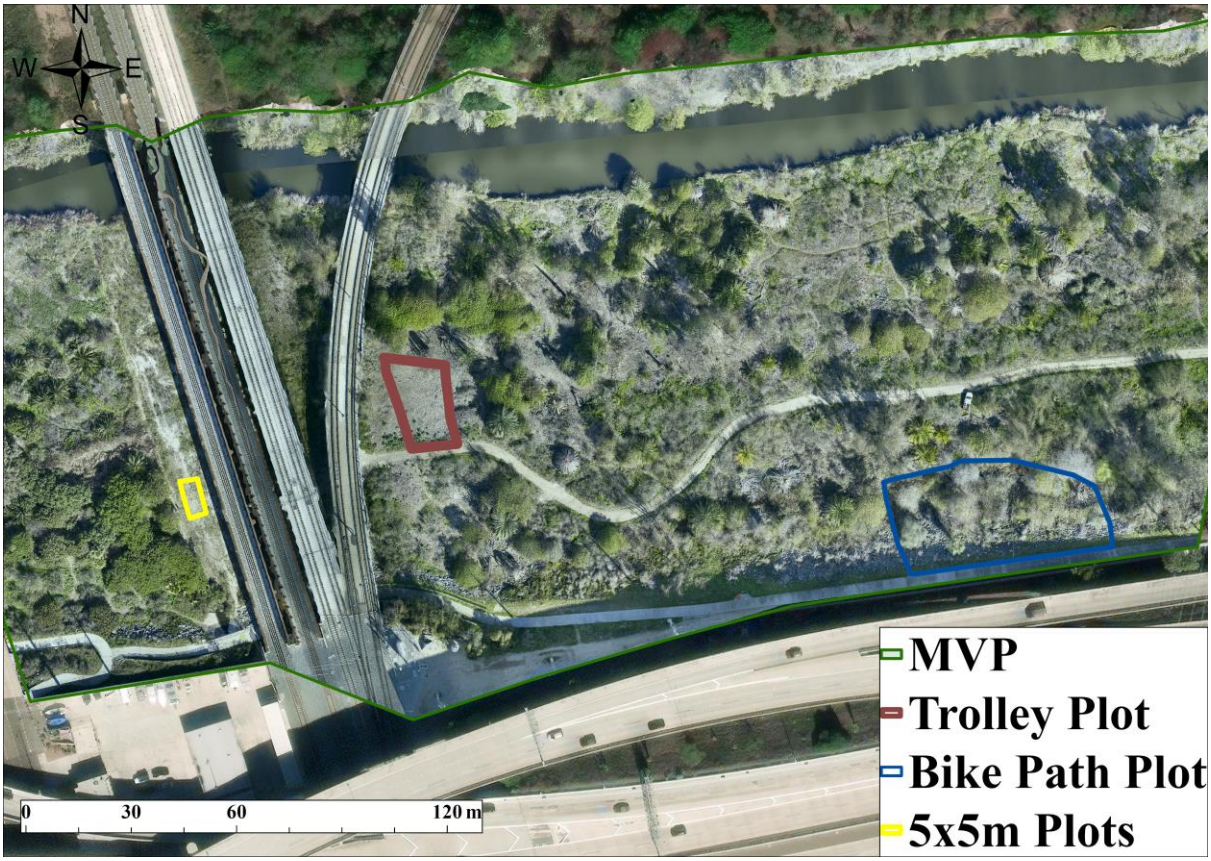


Figure S1. Spatial distribution of ground reference plots used for model training and validation across survey locations and periods. Mission Valley Preserve – February 2022. Plot locations were chosen to capture a variety of debris types, vegetation conditions, and encampment presence to ensure diverse training inputs and robust validation coverage

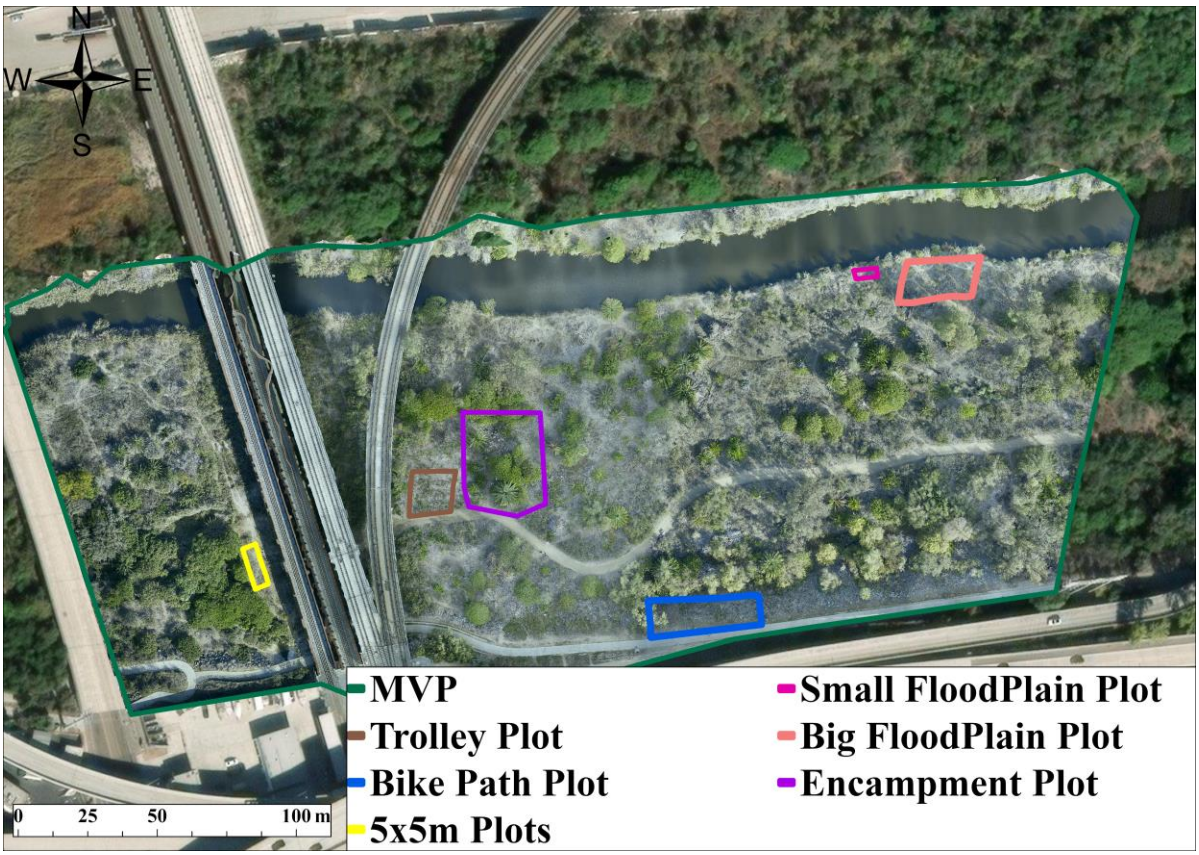


Figure S2. Spatial distribution of ground reference plots used for model training and validation across survey locations and periods. Mission Valley Preserve – October 2022.

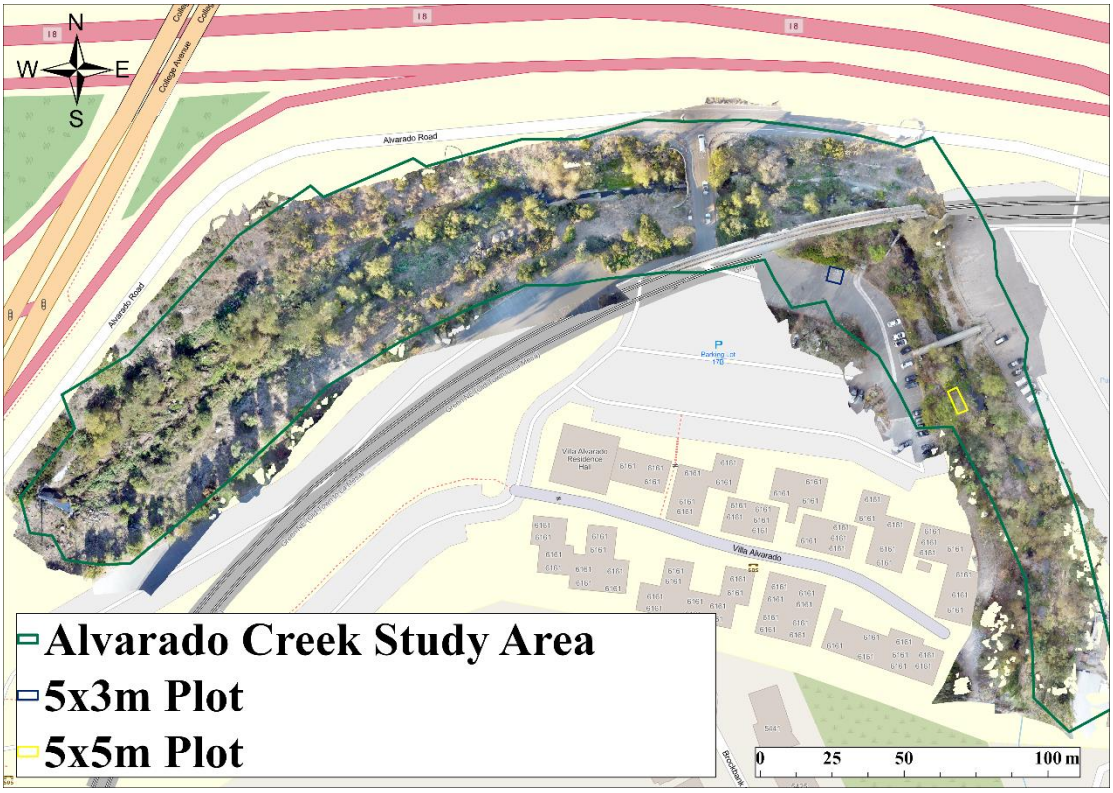
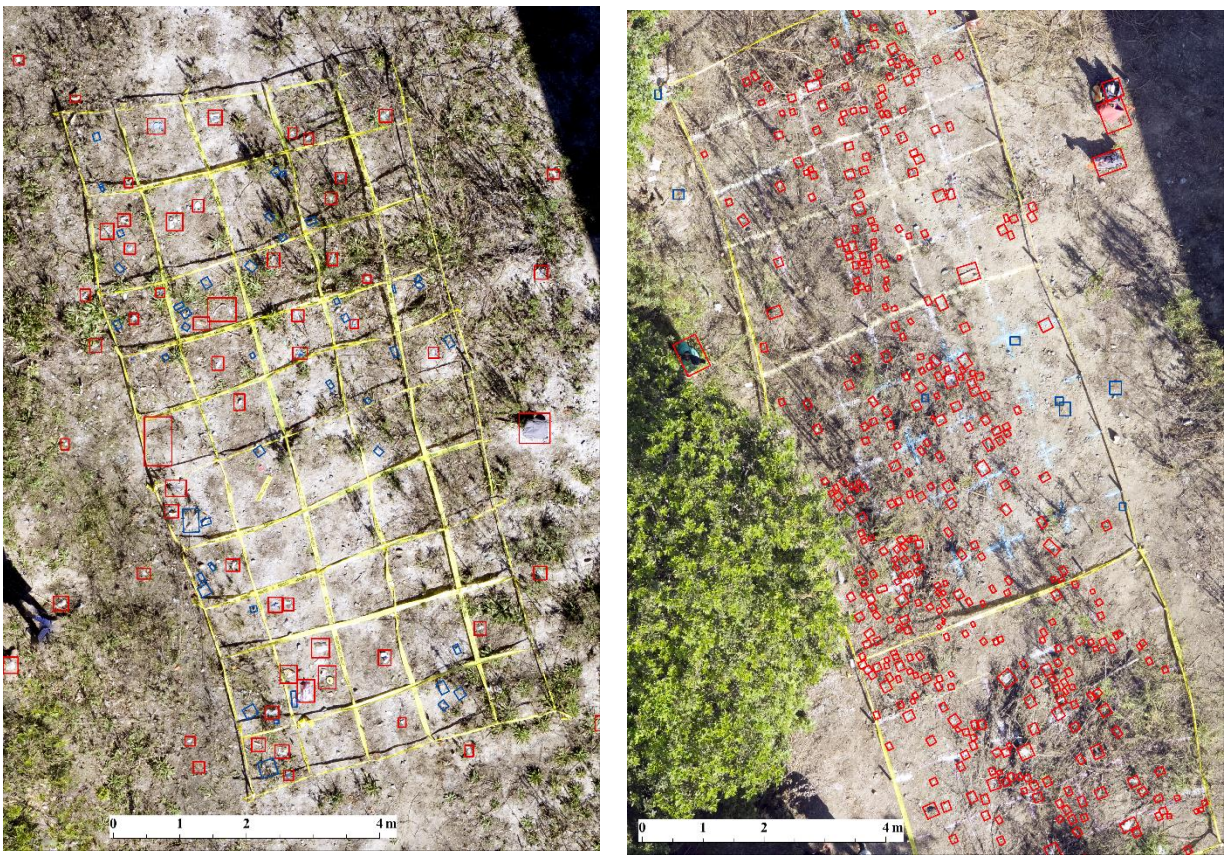


Figure S3. Spatial distribution of ground reference plots used for model training and validation across survey locations and periods. Alvarado Creek – November 2023.

(a)



(b)

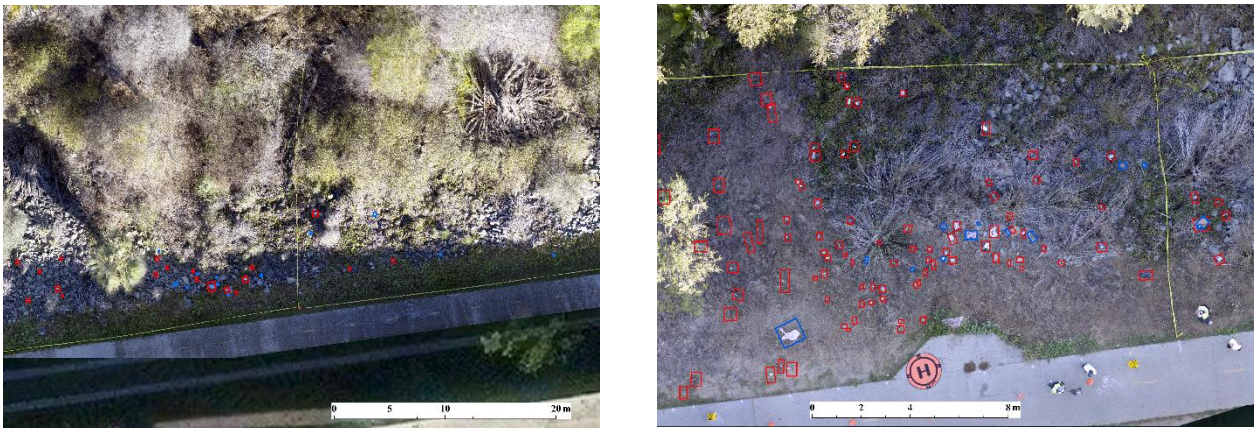
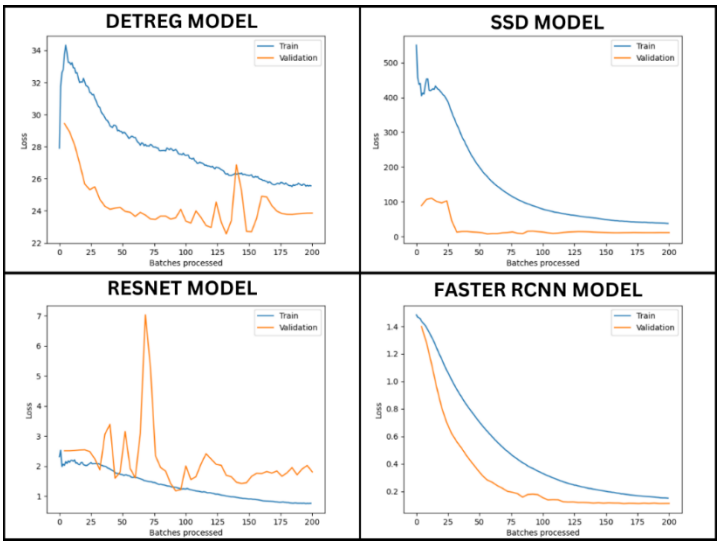


Figure S4. Detection results from the MMDetection model applied to monitoring plots at Mission Valley Preserve. Red boxes indicate predicted debris locations; blue boxes indicate instances where the model failed to predict debris. (a) Detection output for 5×5 m plots, left to right: February 18, 2022, and October 29, 2022 surveys. (b) Detection output for Bike Path plots, left to right: February 18, 2022, and October 29, 2022 surveys.

(a)



(b)

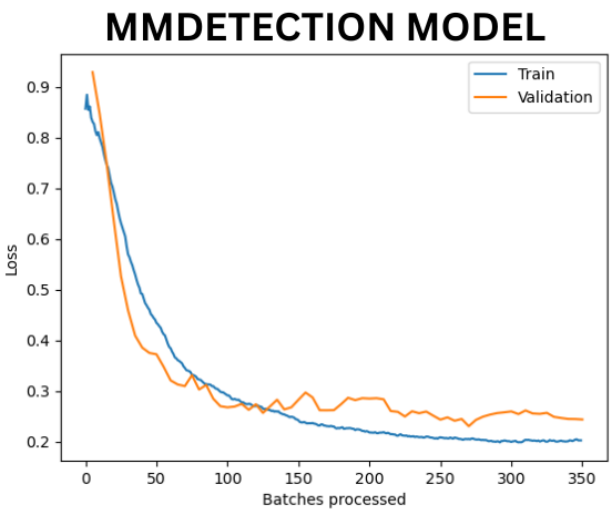
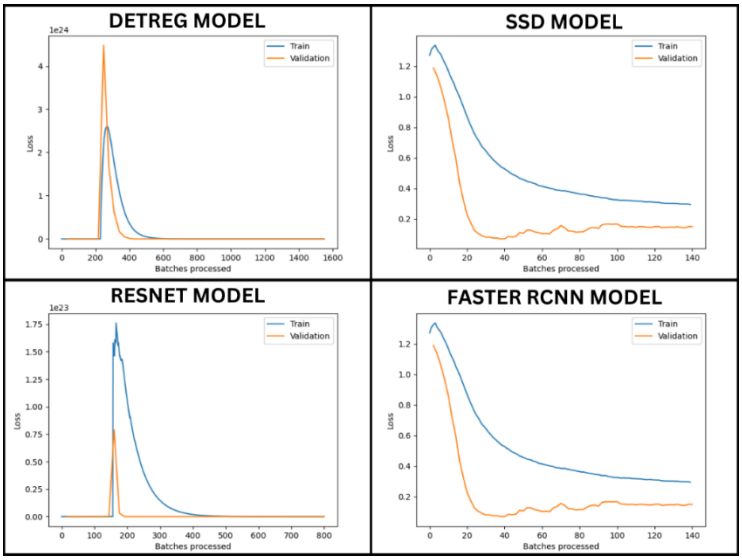


Figure S5. Training and validation loss curves for four deep learning models (DetReg, SSD, RetinaNet, Faster R-CNN) and one ensemble model (MMDetection) on the 5×10 m plot from the February 2022 Mission Valley Preserve survey. (a) Loss curves for DetReg, SSD, RetinaNet, and Faster R-CNN. (b) Loss curve for the MMDetection model using the Cascade R-CNN architecture.

(a)



(b)

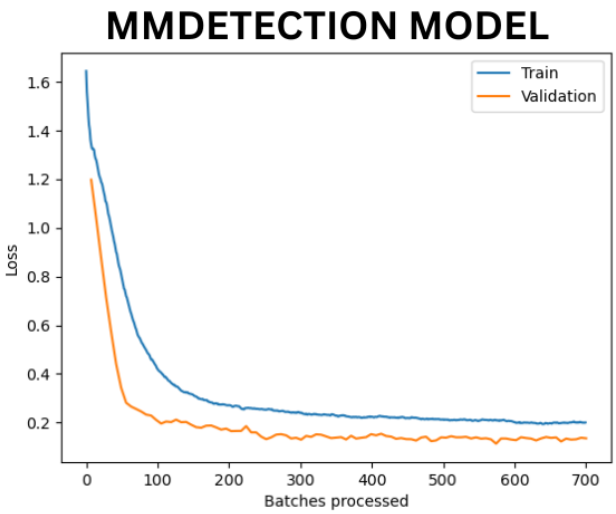


Figure S6. Training and validation loss curves for five models on the 5×15 m plot from the October 2022 Mission Valley Preserve survey. (a) DetReg, SSD, RetinaNet, and Faster R-CNN models. (b) MMDetection with Cascade R-CNN

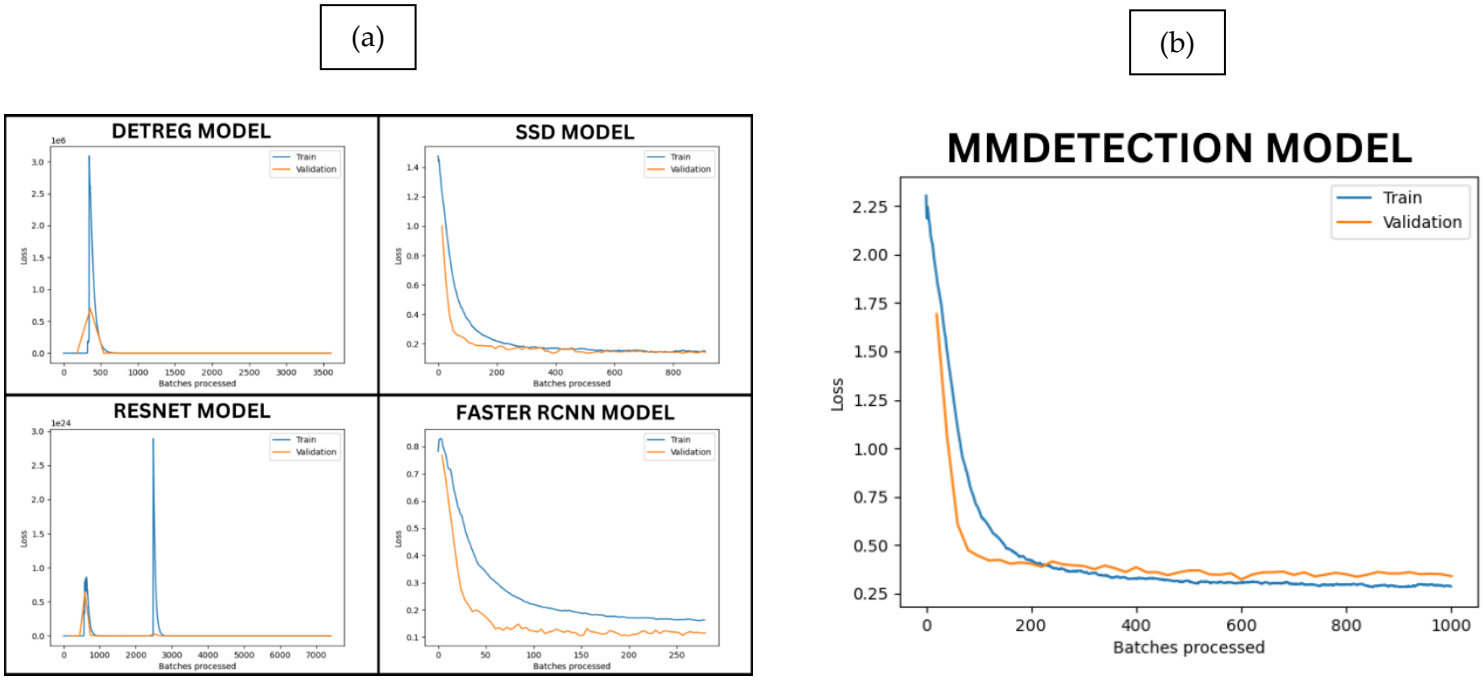


Figure S7. Loss curves showing model training behavior for the Alvarado Creek site. (a) DetReg, SSD, RetinaNet, and Faster R-CNN models. (b) MMDetection model. Loss is plotted against number of training epochs.

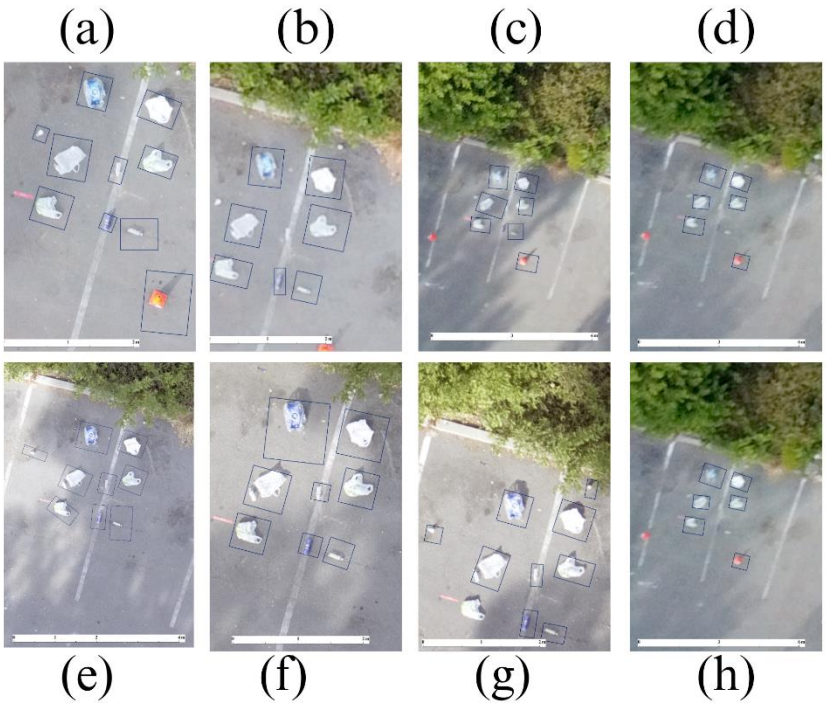


Figure S8. Impact of UAV flight altitude and corresponding image resolution on debris detection accuracy at the parking lot plot. Results are shown for both UAV platforms: (a–d) Mini at altitudes of 100 ft, 200 ft, 300 ft, and 400 ft, respectively; and (e–h) Matrice at matching altitudes. Detection performance declines noticeably with increasing altitude due to reduced spatial resolution, particularly beyond 300 ft.

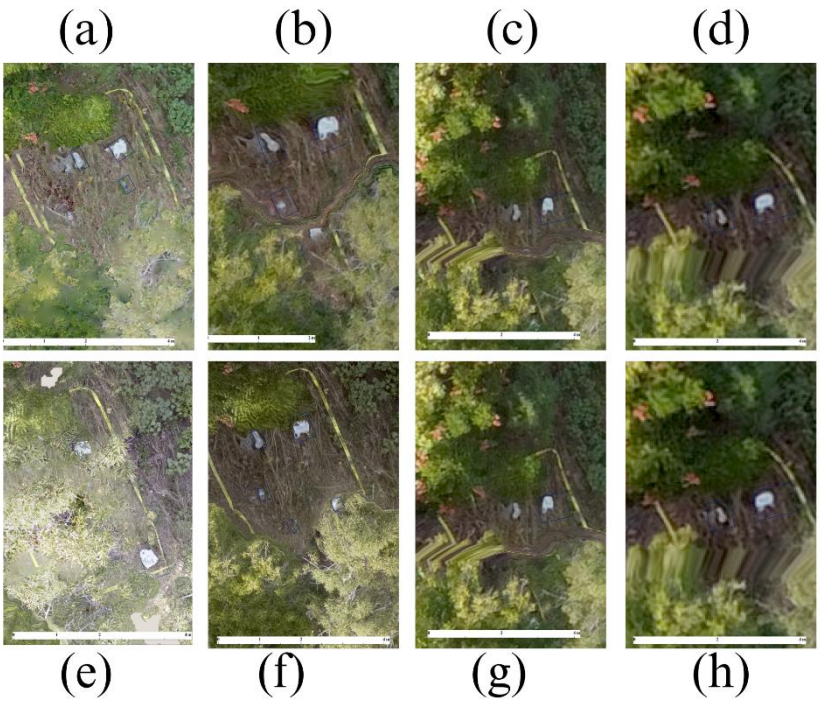


Figure S9. Impact of UAV flight altitude and corresponding image resolution on debris detection accuracy at the floodplain plot. Results are shown for both UAV platforms: (a–d) Mini at altitudes of 100 ft, 200 ft, 300 ft, and 400 ft, respectively; and (e–h) Matrice at matching altitudes. Detection performance declines noticeably with increasing altitude due to reduced spatial resolution, particularly beyond 300 ft.